CHAPTER 5

DESIGN AND SIMULATION INVESTIGATIONS OF DUAL-BAND (S- AND C-BAND) RBWO WITH SECTIONAL SLOW-WAVE STRUCTURES

CONTENTS

* Part of this work has been published as:

V. Venkata Reddy and M.Thottappan, " Design and Simulation Investigations of Dual-Band RBWO Using Sectional Slow Wave Structures for Long Pulse Generation," ***IEEE Transactions on Electron Devices***, vol. 69, no. 10, pp. 5858-5864, Oct. 2022 (10.1109/TED.2022.3201834).

CHAPTER 5: DESIGN AND SIMULATION INVESTIGATIONS OF DUAL-BAND (S-AND C-BAND) RBWO WITH SECTIONAL SLOW-WAVE STRUCTURES

5.1 Introduction

The HPM sources have made significant progress with high conversion efficiency and high average RF output power over a single frequency generation. The extensive application of dual-band/dual-frequencies are space, EM weapons for electronic warfare to target two enemies at a time, plasma heating, and various communication and sounding systems [3]. In recent years, the development of dual-band/dual-frequency HPM sources with a single beam has become very attractive in view of high conversion efficiency, and high average RF output power with a stable and clear RF output power. The main disadvantage of dual-beam/dual-band is beam synchronization and multiplexing of RF output radiation [99]. The advantage of dual-band/dual-frequency (single-beam) RF output power is that it combines the RF output power with a single device and wideband antenna to radiate with low onset time. Dual-band/dual-frequency HPM sources with multiple interaction structures are represented by RBWOs, Magnetrons, Gyrotrons, and MILOs, [99, 150-154]. The HPM sources with single interaction structure (RBWO, Magnetrons, Gyrotrons, Virpertron, Plasma relativistic microwave oscillator, and MILO) can also generate multiple frequencies [7, 42, 73, 115, 155-161]. However, such tunable (single interaction structures) HPM sources cannot generate the RF output power simultaneously with multiple frequencies. Therefore, the dual-band RBWO with sectional SWS's is designed for clear and more stable RF power with a large beating frequency, high efficiency, and exceptionally long pulse duration.

The theory of multi-frequency generation in BWO was first observed by Ginzburg et al. and Carmel et al. [73, 155, 156] with the variation of the operating

current and length of the interaction structure. The RBWO consists of sectional SWS separated by a tapered waveguide supplied by a single beam, and two different transverse diameters of SWS supplied by dual-beam were designed and simulated for obtaining two different bands of frequencies by Wang et al. [43, 100]. Yongfu et al. [162] have designed and simulated coaxial RBWO consisting of both inner and outer SWS operated with dual-beam for dual-band frequency generation. Subsequently, Yongfu et al. [101, 163] have simulated and experimentally tested a coaxial RBWO consisting of a smooth inner waveguide and outer is sectional SWS using a cut-off neck reflector. Further, Yongfu et al. [164, 165] have also simulated and experimentally tested a coaxial RBWO consisting of a smooth inner waveguide, and outer is sectional SWS separated by a tapered waveguide using modulating and asymmetric resonant reflector. Elfrgani et al. [102] have designed a dual-band RBWO using a Bragg reflector for TE_{11} mode output in both C- and X-band frequencies. Recently, Ansari et al. [166] have designed and studied a dual-band (C- and X-band) non-uniform RBWO using a Bragg reflector. In dual-band/dual-frequency RBWO, it is essential to observe how long the individual frequency is being related to the time while generating oscillations. This can be observed by using a time-frequency plot that indicates the time at which frequency generation is "ON" or "OFF". From the above literature, it has been observed that the following gaps are identified in regard to the dual band/dual frequency RBWO: the effect of time-frequency generation by mechanical tuning, frequency generation, and RF power by the voltage tuning of dual-band/dual-frequency have not been reported and the RF output power generation was also reported to 50 ns of simulation time only.

In this chapter, a dual-band RBWO with sectional SWS's has been designed to generate high RF power with a pulse length having a time-frequency generation up to 100 ns. Two slow-wave structures (SWS) are used to generate dual-band microwaves,

and a rectangular resonant reflector (RR) is used to reflect the backward waves generated by both SWS's. The drift section-II separating both SWS's also acts as a reflector, which helps to enhance the pulse duration up to 100 ns of simulation time.

5.2 Design of Dual-Band RBWO with Sectional SWS's

The simulation configuration of dual-band RBWO with sectional SWS's is shown in Figure 5.1. The device is designed in the same transverse dimensions, consisting of a single annular electron beam guided by a strong axial magnetic field 1.3 T. An annular IREB with $r_b / r_0 \approx 0.7$ is propagated axially through two SWS's separated by the drift section-II and finally dumped at the tapered collector region. RBWO is a linear beam device, and the basic principles and theory have been researched for more than five decades. The present dual-band RBWO is also derived from the regular RBWO. The main components of dual-band RBWO with sectional SWS's are (i) SWS-I and SWS-II, (ii) rectangular resonant reflector (RR), (iii) drift section-I, and (iv) drift section-II. The design of each component is given below.

5.2.1 Sectional Slow-Wave Structures (SWS-I and -II)

An S-band SWS (SWS-I) and C-band SWS (SWS-II) are designed with a sinusoidally corrugated cylindrical waveguide profile as given in equations (5.1) and (5.2), respectively,

SWS-1:

$$r_{SWS-I}(\mathrm{z}) = r_{01} + r_{11}\sin(k_1 z), \tag{5.1}$$

SWS-2:

$$r_{SWS-II}(\mathrm{z}) = r_{02} + r_{12}\sin(k_2 z). \tag{5.2}$$

where, r_{01}, r_{02} and r_{11}, r_{12} denote the mean radius and corrugation amplitude of SWS-I and

SWS-II, respectively, and $k_{1,2} = 2\pi / d_{1,2}$ is the wavenumber ($d_{1,2}$ is period of the SWS's). Both SWS's are the heart of the dual-band RBWO, which are used to convert the kinetic energy of the electron beam into microwave energy. The two SWS's have seven uniform periods with the period $d_{1,2} \approx \lambda_{1,2} / 2$. The mean radius of the SWS-I and SWS-II are decided by the ratio $D_{1,2} / \lambda_{1,2}$, where D_1 and D_2 are the mean diameter of the SWS's and $\lambda_{1,2}$ are the microwave operating wavelengths corresponding S- and C-band, respectively. The ratio of D/λ in SWS-I and SWS-II is chosen as ~1 and ~1.35, respectively, in order to obtain a stable RF output power with a long-time duration and a clear frequency spectrum. The corrugation amplitude is chosen using the inequality, $\lambda_{1,2} / 16 \le r_{1,2} \le \lambda_{1,2} / 8$ [63], [117]. The period of the SWS's is determined by the electron energy and must satisfy the Cherenkov condition (phase velocity ≈ beam velocity) of the corresponding operating frequencies. The mean radius and corrugation amplitude determine the minimum and maximum operating frequencies of the passband. The SWS's parameters are calculated as per Chapter 2.4 and listed in Table. 5.1.

The dual-band RBWO with sectional SWS's is designed to operate in the lowest axisymmetric TM_{01} mode to obtain a high coupling impedance. It is beneficial to analyze the interaction and mode of operation for both SWS's by the dispersion relation. The cold dispersion curve shown in Figure 5.2 (black color straight line) is obtained with the theoretical relation given in equation (5.3) without the influence of the beam space charge factor (α = 0).

$$D_{mn}(\omega, k_z) = \left(\frac{\omega^2 - k_m k_n c^2}{\Gamma_n^2 c^2} \right) \times I_{mn}^J \tag{5.3}$$

where, m and n are the model and Floquet's spatial harmonics, k_z and k_m (k_n) are the fundamental and spatial harmonics of the axial wavenumber, Γ_n is the transverse

wavenumber, I_{mn} is the zero-order modified Bessel function, and ω *and* c are the wave operating frequency and velocity of light, respectively. The calculated dispersion is validated by the cold simulation using "CST Microwave Studio", as shown in Figure 5.2 (green color dotted line). The theoretical and simulated dispersions are in good agreement. The intersections of TM_{01} mode with the beam mode line (red color straight line) at ~3.6 GHz for SWS-1 and ~4.5 GHz for SWS-II show the corresponding operating points with the beam energy of ~ 550 keV.

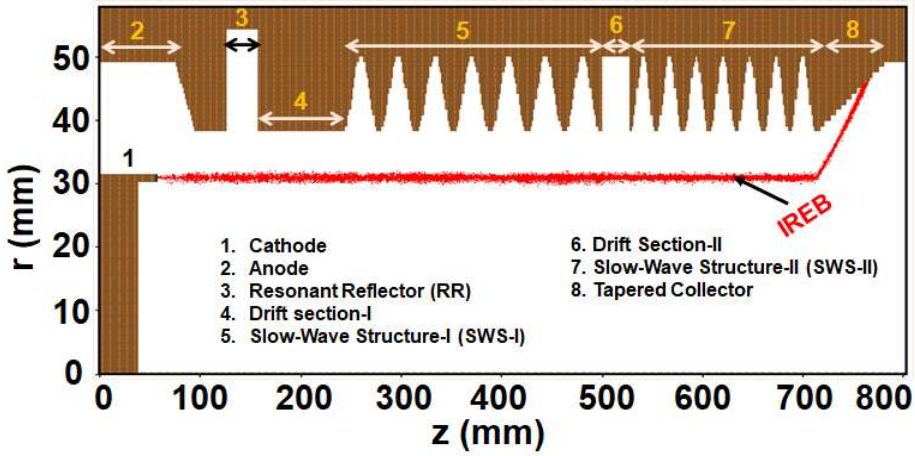

Figure 5.1: 2D simulation configuration of the dual-band RBWO with sectional SWS and IREB particles.

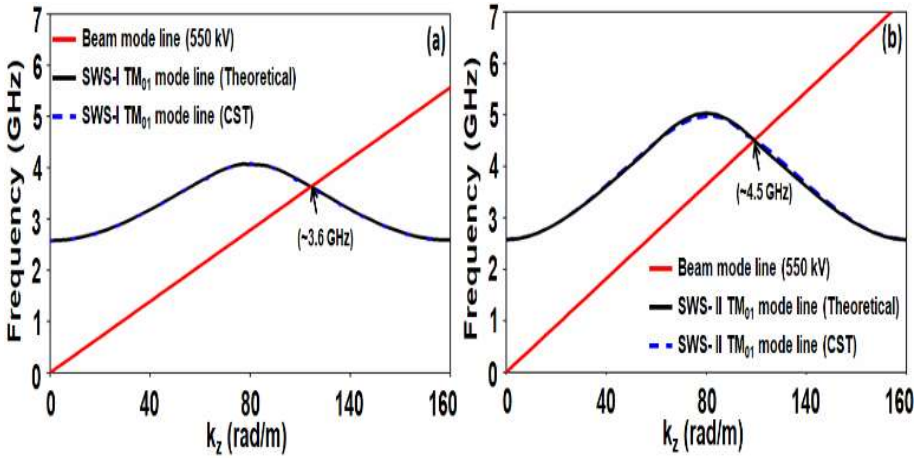

Figure 5.2: Dispersion curve of TM_{01} mode and beam mode line of (a) SWS-I and (b) SWS-II

5.2.2 Rectangular Resonant Reflector (RR)

The RR is designed to extract dual-band RF output power from the cathode end to the

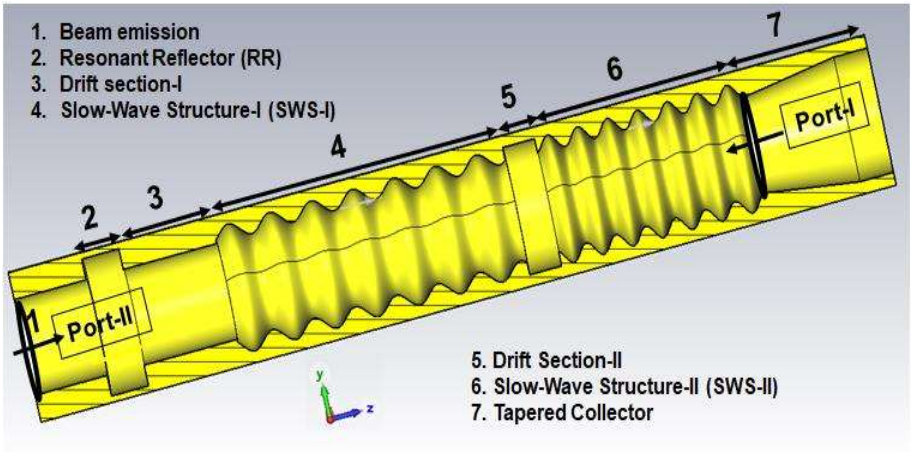

Figure 5.3: CST model of the dual-band RBWO

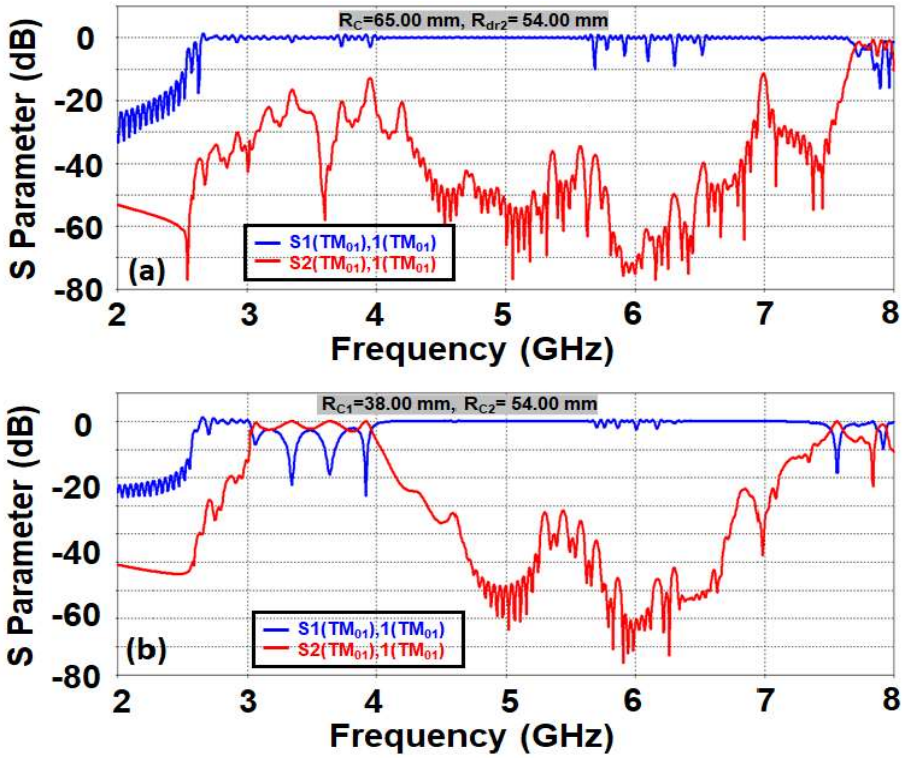

Figure 5.4: Reflection and transmission coefficients of (a) Fig.5.3, and (b) excluding RR in Fig. 5.3.

collector end. This leads forward TM_{01} wave (fundamental harmonic) appearing in the interaction space along with -1st harmonic of the backward TM_{01} wave generated due to Cherenkov synchronization of both SWS-I and SWS-II. To obtain the maximum conversion from the backward -1st harmonic of TM_{01} wave into a forward fundamental harmonic of TM_{01} wave and to lock the next high-order modes, the RR radius and

length are calculated by using, $R_C \approx \chi_{02} / \lambda_1$ and $L_C \approx \lambda_1 / 3$, respectively, where, λ_1 is operating wavelength of SWS-1. The impedance discontinuity of RR (Figure 5.4) is observed by the cold analysis of dual-band RBWO with sectional SWS's (Figure 5.3) by using the finite integration technique based on numerical code. At port-1 TM_{01} mode is applied (i.e., at the end of the SWS-II) to observe the reflection coefficient (at port-1) and transmission coefficient (at port-2). It is observed from Figure 5.4 (a), the TM_{01} mode is fully reflected from 2.6 GHz to 5.6 GHz without any impedance discontinuity and nullifies the transmission coefficient. It shows that the RR acts as a reflector for both bands of frequencies.

5.2.3 Drift Section-I

The drift section between RR and SWS-I is used to adjust the phase between the backward -1st harmonic of TM_{01} wave and the forward fundamental harmonic of TM_{01} wave of both bands to avoid the synchronism and its phase should be 180^0 [7], 167]. Therefore, the radius and length of the drift section-I are calculated by using $L_{dr1} \approx \lambda_1$ and $R_{dr1} < \chi_{02} / \lambda_1$ [168], to favor the desired mode of interaction.

5.2.4 Drift Section-II

The role of drift Section-II is to separate both SWS's and also to play the role like the drift section-1, as explained before. The drift section-II also acts as a reflector for SWS-II along with the RR. The transmission and reflection coefficients of the drift section-II are calculated [Figure 5.4 (b)] through the cold simulation. The effect of drift section-II is observed by leaving the RR section on the device. Figure 5.4 (b) indicates that TM_{01} mode power is reflected from the drift section-II and forwarded towards the collector with the frequency range of 4.0 GHz to 7.4 GHz, only. The design parameters of RR,

drift section-I, and drift section-II are optimized to maximum reflections, as given in Table 5.1.

Table 5.1: Structural Parameters of the Present Dual-Band RBWO.

Parameters		Symbols	Values (mm)
Slow-wave Structure-I (SWS-I)	Mean radius	r_{01}	44.40
	Ripple amplitude	r_{11}	06.07
	Period	d_1	36.80
	SWS length	L_{sws-1}	7*d
Slow-wave structure-II (SWS-II)	Mean radius	r_{02}	44.40
	Ripple amplitude	r_{12}	6.07
	Period	d_2	26.53
	SWS length	L_{sws-II}	7*d
Resonant Reflector (RR)	RR length	L_C	23.50
	RR radius	R_C	65.00
Drift Section-I	Drift length	L_{dr1}	83.00
	Drift radius	R_{dr1}	38.30
Drift Section-II	Drift length	L_{dr2}	25.00
	Drift radius	R_{dr2}	54.00

5.3 PIC Simulation of Dual Band RBWO

The full-wave particle-in-cell (PIC) simulation of the present dual-band RBWO (Figure 5.1) is studied for its beam-wave interaction by using a Finite Difference Time Domain (FDTD) based 3D electromagnetic code. A beam voltage of 550 kV [Figure 5.5 (a)] is applied between the anode and cathode to obtain a beam current of ~5.4 kA [Figure 5.5 (b)]. The instantaneous and average RF output power (Fig. 5.6) are measured at the end of the collector. A stable average RF output power of ~0.6 GW (green color in Figure 5.6) is predicted up to 100 ns of simulation time by filtering the instantaneous RF output power (red color in Figure 5.6) with ~20.20 % conversion efficiency. The axial electric field of the desired TM_{01} mode is developed during the beam-wave interaction, which is

observed using "OBSERVE FIELD_INTEGRAL E. DL" command defined at the end of the tapered collector (Figure 5.7). The frequency spectrum (Figure 5.8) is

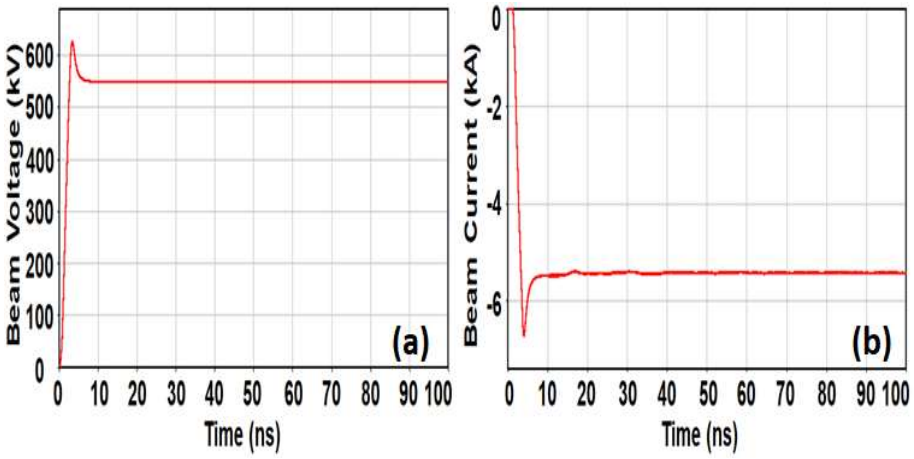

Figure 5.5: a) Applied beam voltage in b/w anode and cathode, and b) Developed beam current at the entrance of SWS-I of the present dual-band RBWO.

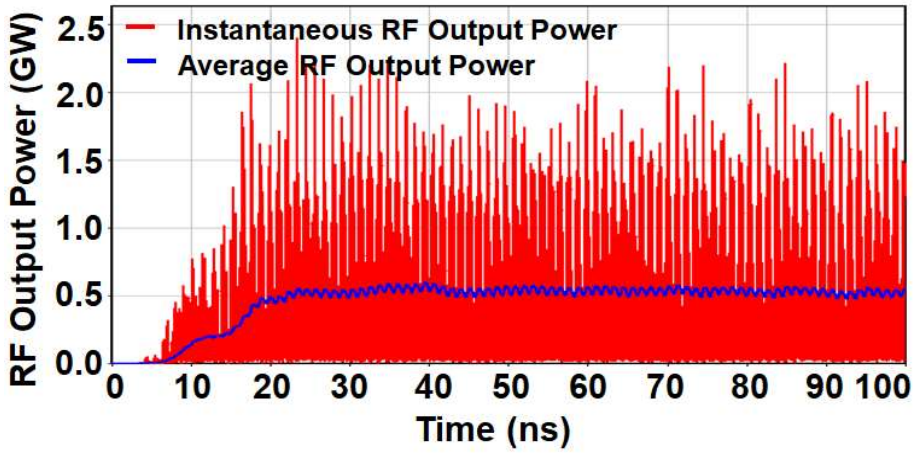

Figure 5.6: Instantaneous and average RF output power of the dual-band RBWO with sectional SWS's.

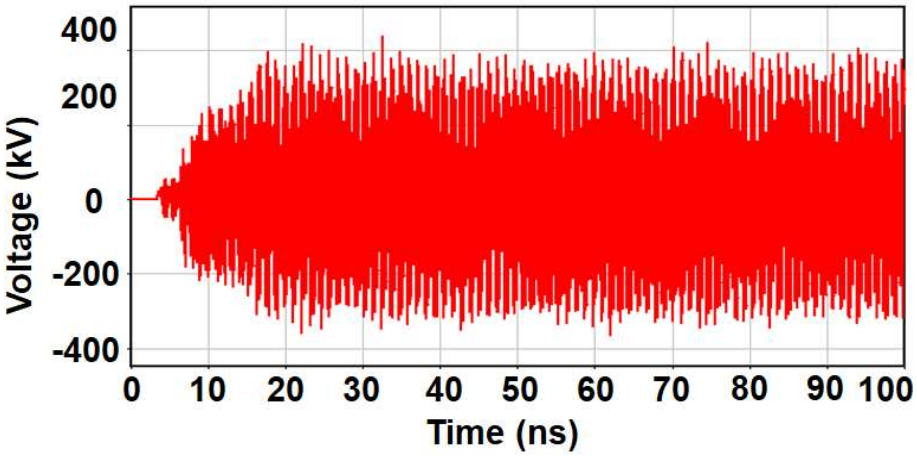

Figure 5.7: Axial electric field integral over a length vs time at the end collector of the dual-band RBWO with sectional SWS.

obtained by applying the Fast Fourier Transform (FFT) command on the obtained axial electric field (Figure 5.7). This gives the operating frequencies of beam-wave interaction of SWS-I and SWS-II, i.e., ~3.6 GHz and ~4.5 GHz, respectively. The first oscillation frequency (~3.6 GHz in Figure 5.8) is obtained due to SWS-I, and the second oscillation frequency (~4.5 GHz in Figure 5.8) is obtained due to SWS-II. The separation of two operating frequencies is ~0.9 GHz, which is called beating frequency. The field pattern is observed at the end of the simulation to confirm the operating mode as TM_{01} (inset of Figure 5.8) and also observed that there are no harmonics, and competing modes are not generated.

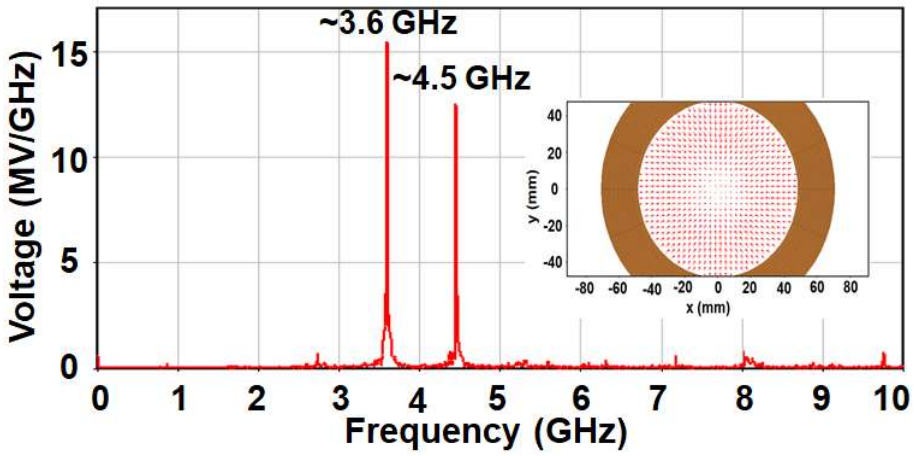

Figure 5.8: The Frequency spectrum of dual-band RBWO with sectional SWS's.

The phase space plot of the particle distribution in the axial direction at a different instance of time is observed (Figure 5.9) by using PHASESPACE axis Z, KE command, where, Z is the axial distance, and KE is the kinetic energy per particle (eV). The particle distribution (bunching) indicates that the electron beam is initiated the interaction from SWS-II and generated C-band microwaves first. After some time, the electron beam is interacted with SWS-II as well as SWS-I and ends at the beginning of SWS-I. The S-band microwave is generated due to the interaction of the electron beam with SWS-I. The beam-wave interaction is uniform and strong in both SWS-I and SWS-

II regions. This helps to generate the dual-band time-frequencies up to 100 ns and generate the RF power up to 100 ns simulation time. The difference in the interaction of the SWS-I and SWS-II w.r.t time and frequency is clearly observed by applying the TIME_FREQUENCY SPECTROGRAM command on the obtained axial electric field (Figure 5.7) for a frequency range of 0 to 10 GHz. This gives the time versus frequency plot (Figure 5.10), which shows that the C-band generation (due to SWS-II) starts at ~6 ns, and S-band generation (due to SWS-I) starts at ~10 ns, and it also gives the beating frequency of ~0.9 GHz. The distribution of the axial electric field (Figure 5.11) in the dual-band RBWO with sectional SWS's obtained with the help of RANGE FIELD Ez command at 100 ns. It shows that the axial electric field in SWS-I and SWS-II is

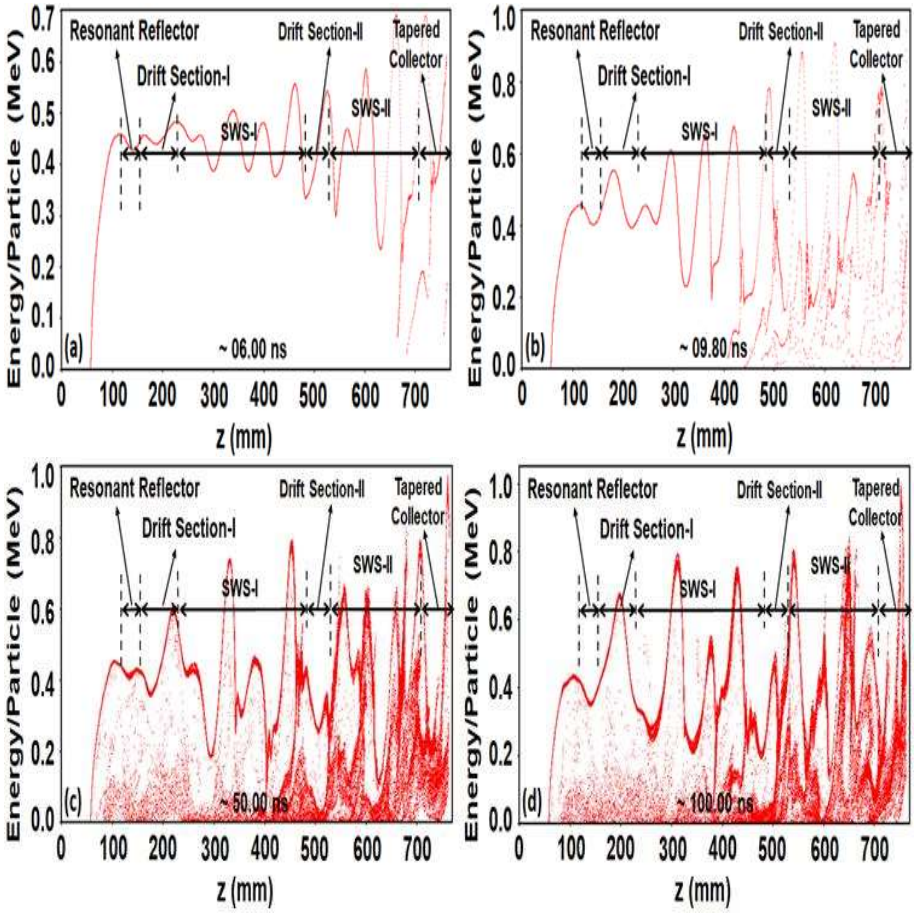

Figure 5.9: Phase-space distribution of electron energy along the axial direction of sectional SWS's at (a) ~6 ns, (b) ~9.8 ns, (c) ~50 ns, and (d) ~100 ns of simulation time (SWS-I region from 250 mm to 500 mm, and SWS-II region from 520 mm to 700 mm).

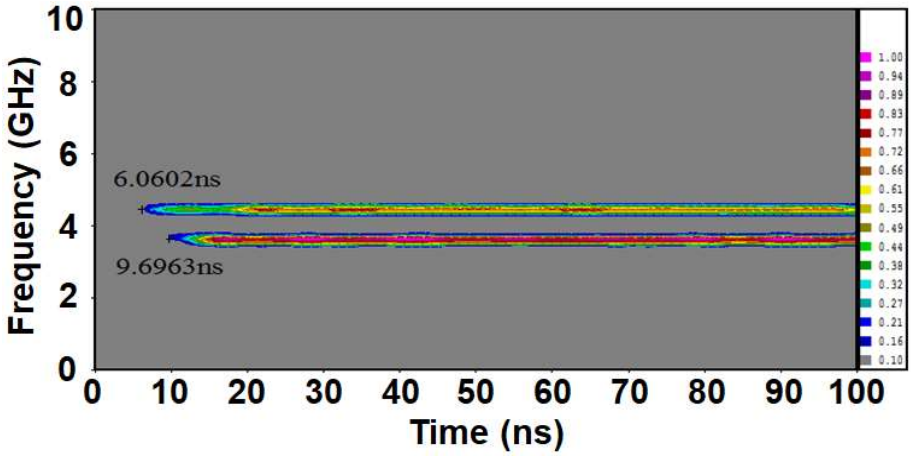

Figure 5.10: Time-frequency spectrogram of the axial electric field (Fig. 5.7).

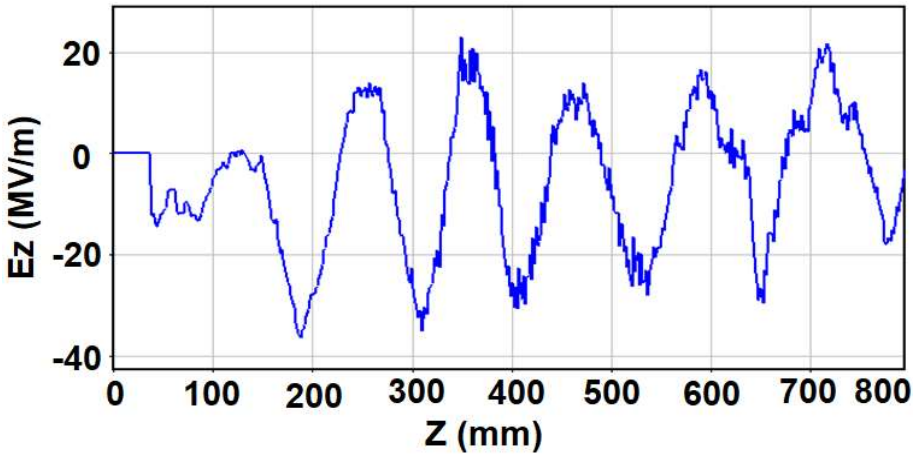

Figure 5.11: Distribution of axial E-field in the present dual-band RBWO.

approximately uniform. This also confirms that the well-modulated bunched electron beam interacts with the same electric field in SWS-I and SWS-II, which converts the DC energy into RF energy continuously up to 100 ns of simulation.

5.4 Parametric Analysis and Discussion

The sensitivity of the device with different design specifications consists of length of drift section-I and drift section-II, magnetic field, and beam voltage are studied.

5.4.1 Effect on frequency generation and RF power by drift section-I and drift section-II (L_{dr1} and L_{dr2})

The effect on the S- and C-band frequencies and its time-frequency generation, and the RF output power can be observed by shifting the drift section-I and drift section-II length (Ldr1 and Ldr2). The variation of Ldr1 and Ldr2 is called as mechanical tuning. The PIC simulation results fully reveal that varying the drift section-I and drift section-II lengths, which significantly affect the frequency generation and its time duration, and the RF output power. The dual-band frequency generation and the time duration of each frequency generation are explained with the help of a time-frequency spectrogram [Figure 5.12 (a)]. As shown in Figure 5.12 (a), the C-band generation and its duration are fully affected , as compared to the S-band generation over a wide range of Ldr1 from 10 mm to 100 mm with a step of 10 mm with the frequency ranging from 2 GHz to 6 GHz. Similarly, Ldr2 over a range of 0 mm to 50 mm is shown in Figure 5.13 (a). Corresponding to the Ldr1 and Ldr2 values, the RF output power (average) is also observed, as shown in Figure 5.12 (b) and Figure 5.13 (b), respectively. The S- and C-band amplitudes [Y-axis in Figure 5.8] also varied for various values of Ldr1 and Ldr2. The intensity of the time-frequency spectrogram of each frequency indicates the variation of amplitudes [Y-axis in Figure 5.8] in the corresponding frequency. If the intensity is high, the frequency amplitude is maximum, and if the intensity is low, the frequency amplitude is low. Both the intensity and amplitude indicate that how the RF output power is strong at the respective operating frequency. The optimum values of Ldr1 and Ldr2 are computed as 83 mm and 25 mm, respectively. The variation of frequency generation, their duration, and RF output power by L_{dr1} and L_{dr2} due to the phase change between the backward and forward wave, and end reflections. The variation of Ldr1 and Ldr2 is called the forward and backward shifting [84, 169, 170].

The drift section-I is placed in between the RR and SWS-1, which acts as a forward shifter for SWS-1 and SWS-II, and the drift section-II is placed between the SWS-1 and SWS-II, which acts as a backward shifter for SWS-I and forward shifter for SWS-II. The end reflections and phase change between the fundamental forward wave and -1st

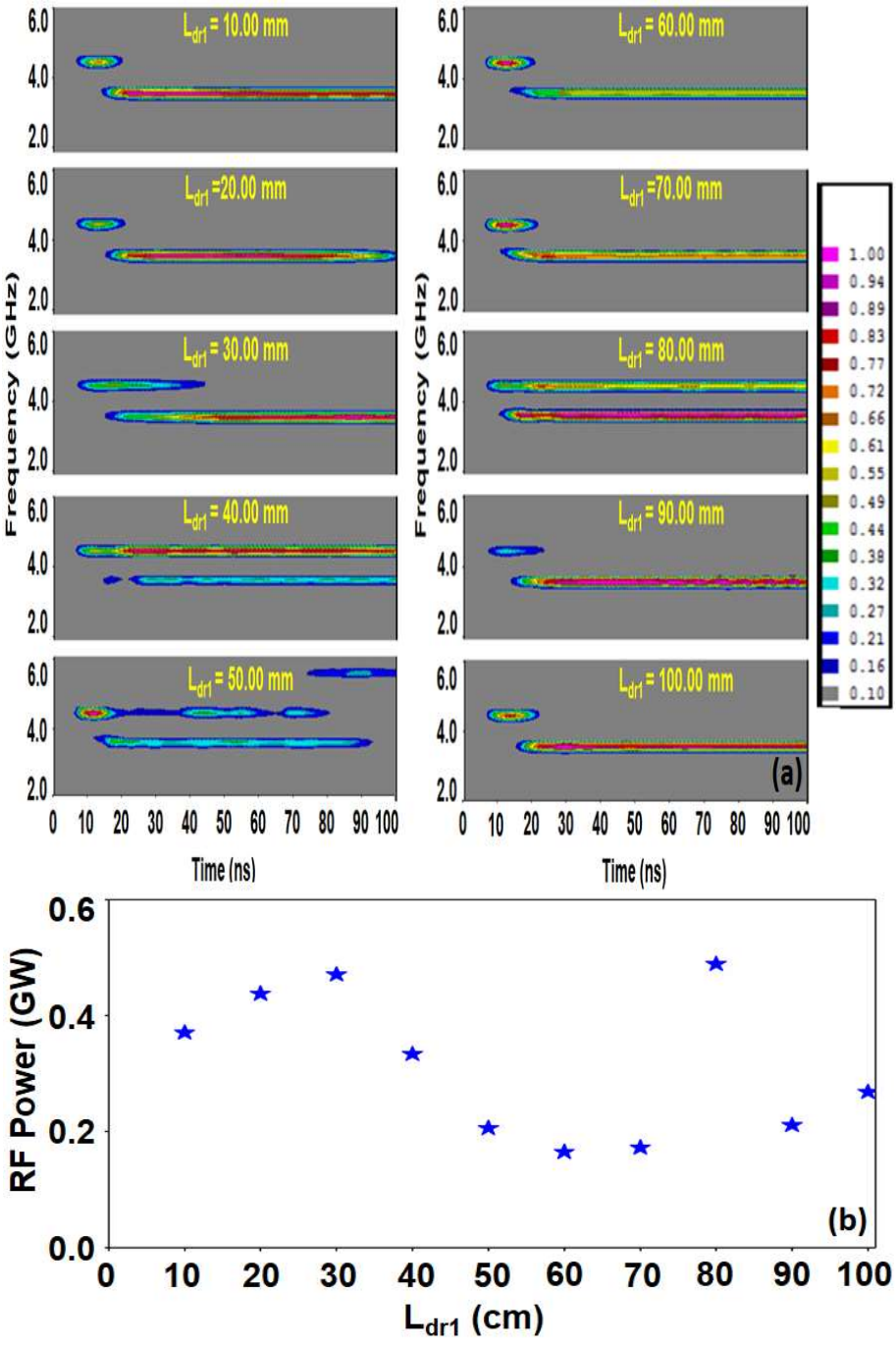

Figure 5.12: Effect of drift section-I length on (a) time-frequency spectrogram and (b) RF power.

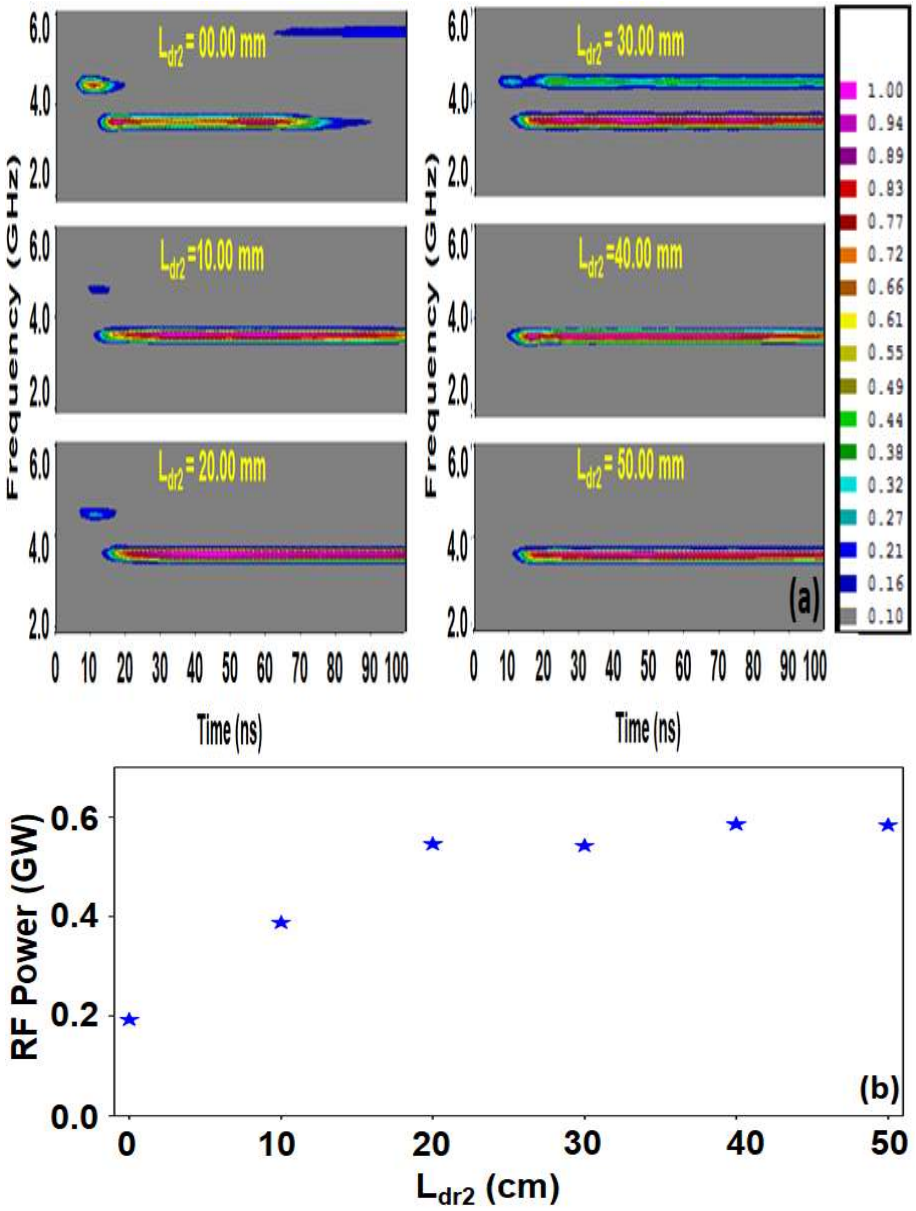

Figure 5.13: Effect of drift section-II length on (a) time-frequency spectrogram and (b) RF power.

harmonic of the backward wave of SWS-I and SWS-II are changed by Ldr1 and Ldr2. The variation of Ldr1 and Ldr2 also causes the degradation of the electron beam quality (energy of the electron beam scattered), which affects the beam-wave interaction in SWS-II.

5.4.2 Effect on frequency and RF power by DC magnetic field

In a regular RBWO, the RF generation is suppressed in the region (i) and region (ii) due

to cyclotron and Cherenkov absorption [125]. In the present configuration, the RF generation is suppressed in the region (i) due to cyclotron absorption [Figure 5.14 (a)]. However, the RF generation is not suppressed in the region (ii) due to Cherenkov absorption, which does not occur simultaneously in both S-and C-bands [Figure 5.14 (a)]. Therefore, the RF power is continuously generated even if any one of the bands is under Cherenkov absorption [Figure 5.14 (b)]. The dual-band frequency generation and average RF output power were observed by varying the magnetic field from 0.1 T to 1.3 T (Figure 5.14). The dual-band generation is commenced from 0.2 T [Figure 5.14 (a)] and below that value, the dual-band generation is absent due to cyclotron absorption. Further, the S-band generation is absent from 0.38 T to 0.45 T, and the C-band

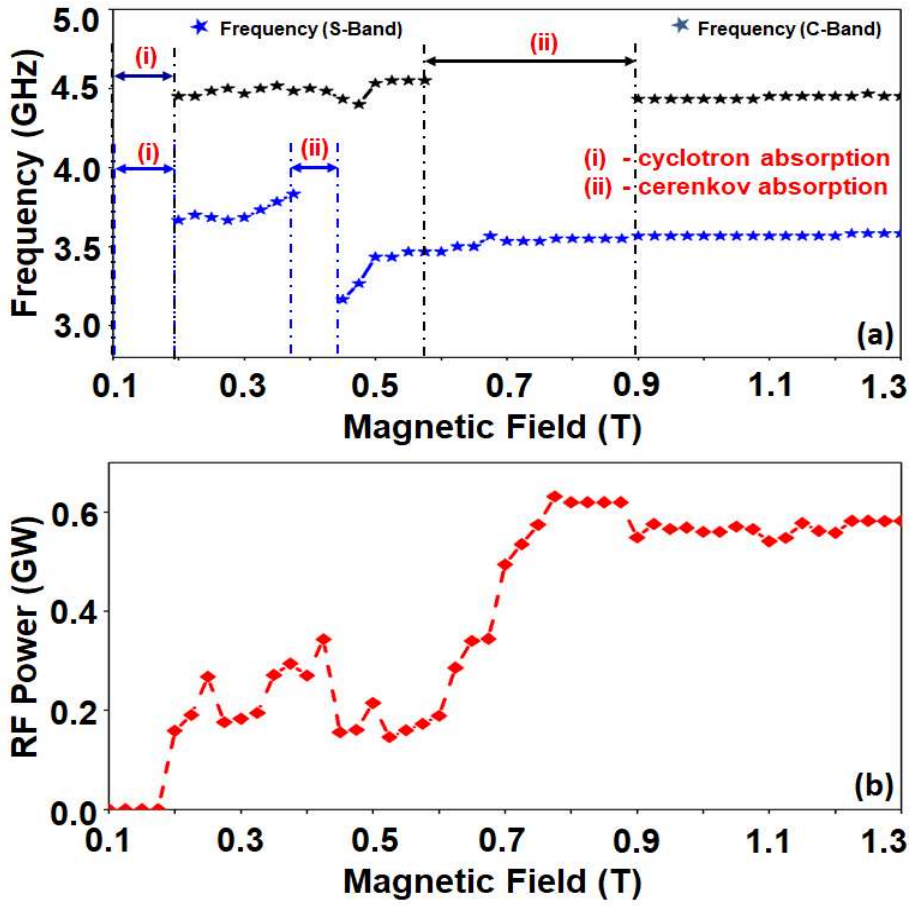

Figure 5.14: Effect of guiding magnetic field on (a) dual-band frequency generation and (b) RF power.

generation is absent from 0.58 T to 0.90 T [Figure 5.14 (a)], which is caused by Cherenkov absorption. The simulation of Cherenkov and cyclotron absorption magnetic field values are good in agreement with theoretical values, as explained in [125]. The dual-band frequency generation with high RF output power consists of time-frequency generation up to 100 ns simulation (Figure 5.6, Figure 5.8, and Figure 5.10) achieved at 1.3 T, as shown in Figure 5.14 (b).

5.4.3 Effect on frequency and RF power by beam voltage

RBWO is better known as a tunable voltage source. The voltage tunability of the present dual-band RBWO with sectional SWS's is observed by varying the voltage applied between the anode and cathode of the device (Figure 5.1). As the voltage varies from 300 kV to 700 kV, the RF output power is increased from ~0.06 GW to ~0.8 GW (Figure 5.15). As the voltage increases above 700 kV, the RF power is decreased due to the shift in the operating point, i.e., ~π-point. However, the operating frequencies in both S- and C-bands are observed for the beam voltage from 300 kV to 900 kV (Figure 5.15). Therefore, the simulation of the present RBWO predicted that the dual-band RBWO with sectional SWS's could also be tuned and used as a tunable source over the range of DC beam voltage.

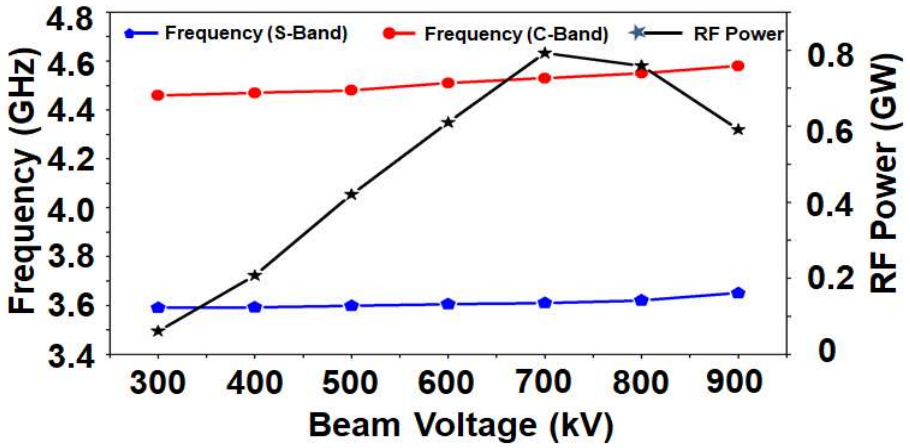

Figure 5.15: Effect of beam voltage on a) dual-band frequency and (b) RF power. range of DC beam voltage.

5.5 Conclusion

An RBWO consists of sectional SWS's separated by a drift section (drift section-II) with RR has been designed and studied to generate the dual-band microwave generation with high power and dual-band time-frequency generation up to 100 ns of pulse length. The RR has been designed to reflect both bands of microwaves. The length of the drift section-II influences the microwave generation and RF output power, and it acts as a reflector for the C-band. Both S- and C-band signal started generating at ~10 ns and ~6 ns, respectively, and the pulse generation at both bands continued up to 100 ns of simulation time without any pulse shortening. The effect of drift section-I (Ldr1) and drift section-II (Ldr2) on the RF output power, and frequency and its time-frequency generation in both S-band and C-band were studied. The simulation results predicted that the frequency generation has not been greatly affected by mechanical tuning. However, the frequency generation had a much impact over the time duration. The frequency generation time is very important in HPM generation especially in dual-band/frequency to radiate the RF power in both bands. Further, the effect of the magnetic field upon the frequency generation of each band and its RF output power was also studied. Finally, the tuneability of the present dual-band RBWO was also studied.

The next Chapter deals about a dual-band operation of RBWO using Bragg reflector for the direct generation of linearly polarized Gaussian like TE11 mode.